



OPEN

## Vacuum curette lumbar discectomy mechanics for use in spine surgical training simulators

Trevor Cotter<sup>1,2</sup>, Rosaire Mongrain<sup>1</sup> & Mark Driscoll<sup>1,2</sup>✉

Simulation in surgical training is a growing field and this study aims to understand the force and torque experienced during lumbar spine surgery to design simulator haptic feedback. It was hypothesized that force and torque would differ among lumbar spine levels and the amount of tissue removed by  $\geq 7\%$ , which would be detectable to a user. Force and torque profiles were measured during vacuum curette insertion and torsion, respectively, in multiple spinal levels on two cadavers. Multiple tests per level were performed. Linear and torsional resistances of  $2.1 \pm 1.6$  N/mm and  $5.6 \pm 4.3$  N mm/ $^\circ$ , respectively, were quantified. Statistically significant differences were found in linear and torsional resistances between all passes through disc tissue (both  $p = 0.001$ ). Tool depth ( $p < 0.001$ ) and lumbar level ( $p < 0.001$ ) impacted torsional resistance while tool speed affected linear resistance ( $p = 0.022$ ). Average differences in these statistically significant comparisons were  $\geq 7\%$  and therefore detectable to a surgeon. The aforementioned factors should be considered when developing haptic force and torque feedback, as they will add to the simulated lumbar discectomy realism. These data can additionally be used inform next generation tool design. Advances in training and tools may help improve future surgeon training.

Virtual-reality (VR) simulation training is an essential tool in training techniques for fields ranging from aviation to driving and beyond<sup>1–5</sup>. Simulators have been able to identify operator skill levels and are required in some cases before professionals are allowed to perform their duties<sup>6–8</sup>. Recent computational and simulation advances have enabled these tools to reach more industries, each with unique challenges. In medicine, the complex nature of the human body, as well as the risks associated with surgery, mean simulators have the potential to revolutionize the way surgeons prepare for procedures<sup>9,10</sup>.

**Surgical simulation.** Surgery carries many dangers, thus the importance of effective surgeon practice and training is evident. Traditionally, surgeons have undergone a combination of classroom, animal, and cadaveric surgical training before approaching a living patient<sup>2,11,12</sup>. However, each of these training methods have limitations such as inaccurate anatomy or physiological response<sup>2</sup>. Alternatively, simulators with various degrees of complexity have been developed to train surgeons on a variety of procedures, from analog laparoscopic knot tying to full VR brain tumor resection<sup>13,14</sup>. The addition of robotic haptic, or touch, devices has enabled these simulators to become more adaptable by removing disposable components such as synthetic tissues and using robotic components to communicate the feeling of them consistently with minimal maintenance<sup>2</sup>. The demand for this type of training is evident by the numerous simulators that have been developed for spine surgery alone<sup>2,15–18</sup>. However, simulators using this technology may require tissue testing and an understanding of the biomechanics of the procedure.

Robotic haptic feedback must communicate the sensations a surgeon encounters during a procedure. This can be broken into two categories: the force and torque present in the procedure, and the force and torque felt by the surgeon.

**Tissue mechanics.** Many techniques exist to mechanically characterize tissues. Properties such as elastic modulus and tensile strength can be derived from tests that measure force or torque and linear or angular displacement on a mechanical tester<sup>19,20</sup>. While this equipment is often limited to one or two axes, multiple tests can be used to generate a multi-axial characterization of the tissue<sup>21,22</sup>. Destructive tests often result in complex

<sup>1</sup>Musculoskeletal Biomechanics Research Lab, Department of Mechanical Engineering, McGill University, Montreal H3A 0C4, Canada. <sup>2</sup>Orthopedic Research Laboratory, Montreal General Hospital, Montreal, QC H3H 1V8, Canada. ✉email: mark.driscoll@mcgill.ca

tissue mechanics. For needle insertion, existing studies have considered the total force  $f_{needle}$  to be the sum of the tissue deformation ( $f_{stiffness}$ ), friction ( $f_{friction}$ ), and cutting ( $f_{cutting}$ ) forces, which are dependent on position,  $x^{23}$ :

$$f_{needle}(x) = f_{stiffness}(x) + f_{friction}(x) + f_{cutting}(x) \quad (1)$$

**Human perception of force.** The mechanical understanding of biological tissues can be used to inform a robot to communicate the tissue force to a user. However, this communication must consider the boundaries of human perception. The just-noticeable difference (JND) is a measure of the minimum perceptible change in force. Hands and fingers are extremely sensitive to the sense of touch, and it has been found that intentional training can improve surgeon skills<sup>24–26</sup>. A JND of [5, 10]% change has been observed during [2, 10] N loads between fingers or in elbow extension, but can vary based on finger, training, and frequency<sup>27–30</sup>. Work on haptic devices has found higher JNDs, including  $23 \pm 13\%$  and  $34 \pm 24\%$  detectable changes for force and torque on the ranges of [0.4, 8.8] N and [20, 410] N mm, respectively<sup>31</sup>. While existing literature shows a wide range of observed JNDs, it is necessary to consider this sensitivity when determining how users will interpret differences in simulated tissue.

**Spinal mechanics studies.** Spinal orthopedic procedures are of particular interest in new surgical simulators<sup>2</sup>. The spine is made up of alternating rigid vertebra and flexible intervertebral discs (IVDs) to create a flexible, supportive structure that protects the spinal cord, cauda equina and other anatomies. Over time or due to injury, IVDs can become compressed or deform, affecting the nerve root exiting from the cauda equina and causing intense pain<sup>32–34</sup>. Treatment of back pain is of immense importance, as it affects 80% of people at some point in their lives and is the leading cause of disability in the world<sup>35,36</sup>. Many treatment options for this pain exist, but the present work focuses on one surgical intervention: lumbar interbody fusion (LIF)<sup>37</sup>.

A LIF procedure aims to relieve pressure on the exiting nerve from the cauda equina. A surgeon performs a discectomy, or removal of the IVD. The surgeon then uses a curette to remove the nucleus pulposus and prepare the endplates of the IVD. With a gap now created, an interbody cage may be placed where the collapsed IVD had been. Bone graft is added at the interbody cage to fuse the two adjacent vertebrae at an appropriate spacing. Finally, pedicle screws and rods are placed to maintain the stability of the vertebrae during healing.

Like many other surgical procedures, modern developments have improved LIF, yielding minimally invasive (MI) procedures. MI surgeries have been found to decrease hospital stays and recovery times<sup>37–39</sup>. As such, a new vacuum curette was developed (Concorde Clear MIS Discectomy Device; DePuy Synthes; Boston, USA) to allow surgeons to perform discectomies with a single tool faster and safer than existing curettes<sup>40</sup>. The adoption of a novel tool requires training. In a surgical simulator context, this also requires the characterization of force and torque encountered when using this tool.

Biomechanical studies performed on the IVD have traditionally been focused on various loading scenarios a person may encounter<sup>41–44</sup>. Few studies deal with the force as surgeons encounter them during surgery<sup>45</sup>. While the known biomechanical properties of the IVD may predict spine behavior under loading, they may be inadequate in predicting mechanical interactions with surgical tools. The unique shape, cutting surfaces, and vacuuming effect of the Concorde Clear may yield unpredictable biomechanical responses. As a result, this work compares peak force and torque, which are the aggregate of stiffness, friction, cutting, and other factors during tool insertion as shown in Eq. (1). Similarly, resistance for each of these quantities is defined by the change of each quantity during loading. Therefore, linear resistance is N/mm and torsional resistance is N mm/°.

This manuscript hypothesizes that discectomy force and torque will be dependent on spinal level and removed tissue at a  $\geq 7\%$  difference, a magnitude detectable to a surgeon. This data can then be used to inform haptic feedback in relevant surgical simulators while drawing attention to the importance of such model selection in other biomechanical studies of the disc.

## Materials and methods

Mechanical testing was performed on human tissues to characterize linear and torsional movements. These data were then analyzed and compared to understand how they differ between anatomical and procedural conditions.

**Sample preparation.** Two fresh frozen cadaveric torsos were acquired from Science Care, Inc. (Phoenix, USA) and tested with ethical approval (McGill University Faculty of Medicine Institutional Review Board (IRB) A04-M13-18A) in accordance with all relevant guidelines, regulations, and consent requirements. Both samples had no history of radiation treatment or spinal surgery. X-rays were used to measure the height of each lumbar IVD to indicate IVD degeneration. Specifications for the cadavers can be seen in Table 1. All IVD height measurements were taken from El-Monajjed et. al, who used the same specimens and methods for preparation<sup>45</sup>. Cadavers were stored at  $-20^{\circ}\text{C}$ , thawed for 5 days at  $2^{\circ}\text{C}$ , and held at room temperature for 72–96 hours before testing. A  $30 \times 30$  cm posterolateral window was removed from the skin, fascia, and muscle to expose the posterior lumbar spine. A  $1 \times 1$  cm annulotomy was performed posterolaterally to gain access to the IVD as would be done in an MI LIF.

**Testing setup.** A custom jig supported the cadaveric torso. The torso was laid on its chest and rotated to allow a linear tester to penetrate at approximately  $40^{\circ}$  lateral to a fully posterior approach. Testing was performed with an MTS 858 Mini-Bionix II testing apparatus and a force and torque load cell of 2.5 kN and 25 N m, respectively (662.20D-01, MTS Systems Corporation; Minneapolis, USA). Custom fixturing connected the tester to one of two tools (Fig. 1).

Cadaveric torso properties					
Cadaver				C1	C2
Gender				M	M
Age				63	69
Height			cm	175	178
Weight			kg	73	86
Collapsed Disc				None	L <sub>4</sub> L <sub>5</sub>
IVD Dimensions	L <sub>1</sub> L <sub>2</sub>	Height	mm	10.0	5.2
		Width	mm	44.7	49.4
	L <sub>2</sub> L <sub>3</sub>	Height	mm	10.3	7.6
		Width	mm	46.1	45.7
	L <sub>3</sub> L <sub>4</sub>	Height	mm	11.6	5.7
		Width	mm	47.6	60.6
	L <sub>4</sub> L <sub>5</sub>	Height	mm	10.3	3.1
		Width	mm	54.1	NA

**Table 1.** Cadaveric torso properties. The cadaver measurements are from a previous work<sup>45</sup>. IVD width is the lateral width.

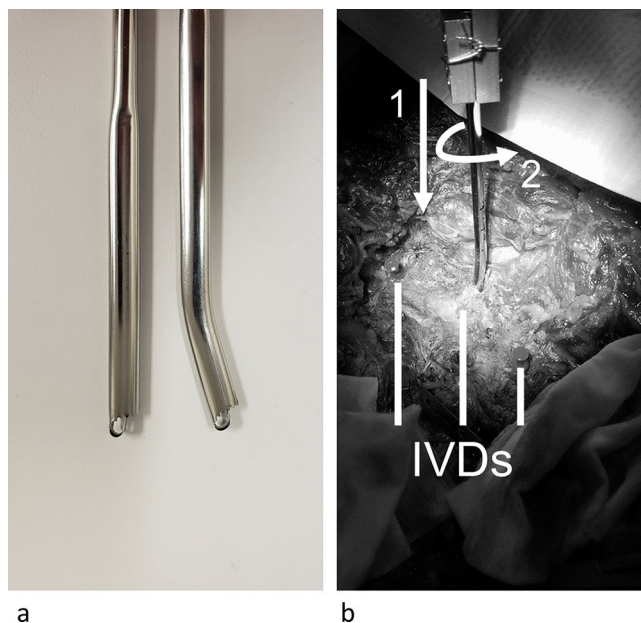


**Figure 1.** Concorde Clear tools used in the test. (a) shows the straightened tool (left) used in the linear test as well as the normal bent tool (right) used in the torsional test. (b) shows the test setup and motion, where the tool is inserted (1) into the intervertebral disc (IVD) and twisted (2). The linear test involved motions 1 and 2, while the torsional test was only motion 2. IVDs are marked.

**Linear testing.** The first test was a linear insertion that mimicked a surgeon penetrating the IVD. The load cell was secured to a straightened version of the Concorde Clear shaft tip, shown in Fig. 1a. The shaft tip was lowered to 5 mm inside the IVD space before beginning. The shaft tip was then inserted at a rate of 0.25 mm/s from [12–15] mm of tool travel, depending on disc size. Meanwhile, the tool was rotated [ $\pm 20$ ]° at 20°/s to prevent snagging and ensure penetration into the IVD. The tool was then withdrawn at the same rates until it returned to its starting position. The tool path can be seen in Fig. 1b, where motions 1 and 2 were performed. Time, position, force, angle, and torque were all recorded at 100 Hz. An example of the position and force results can be seen in Fig. 2a. The test was performed 3 times on the left and right sides of lumbar IVDs between L<sub>1</sub> and L<sub>5</sub>. Additional speed studies were also performed. Linear speeds of 0.25, 0.50, 0.75, and 1.00 mm/s were compared on the right side of C1 L<sub>3</sub>L<sub>4</sub>. Torsional speeds of 10, 20, 30, and 40°/s were compared on the right side of C1 L<sub>4</sub>L<sub>5</sub>. Test details are shown in Table 2.

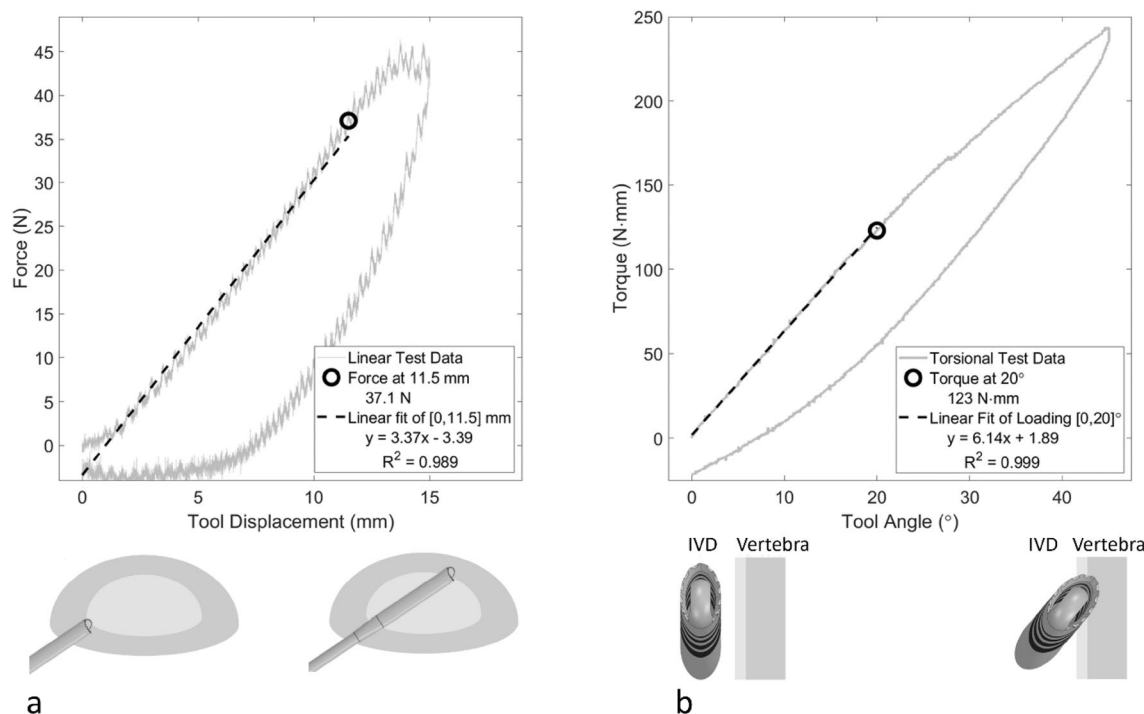


**Figure 2.** Examples of linear (a) and torsional (b) tests with extracted peak and resistance values for the first trial of the right side of C2 L<sub>3</sub>L<sub>4</sub>. The torsional test was performed at a 5 mm depth. Schematics of the tool orientation within the intervertebral disc (IVD) are shown.

Testing parameters			
Test name		Linear test	Torsional test
IVD levels		L <sub>1</sub> L <sub>2</sub> -L <sub>4</sub> L <sub>5</sub>	
Sides		Left and Right	
Linear motion	Waveform	Triangle	NA
	Starting position	5 mm inside IVD	NA
	Range	0-12/15 mm	NA
	Speed	0.25 mm/s	NA
	Additional speed tests	0.50, 0.75, 1.00 mm/s	NA
Torsional motion	Waveform	Sinusoidal	Sinusoidal
	Starting position	0°	0°
	Range	± 20°	± 45°
	Speed	40°/s	2°/s
	Additional speed tests	20, 60, 80°/s	3, 4, 6, 8°/s
Number of Trials		3	5

**Table 2.** Testing parameters.

**Torsion testing.** The second test was a torsional motion that mimicked a surgeon twisting inside the IVD space. The load cell was secured as for the linear test but with an angled Concorde Clear shaft tip, shown in Fig. 1a. The shaft tip was lowered to 5 mm inside the IVD space and twisted at 2°/s to [± 45]° for a total of 5 full cycles. One cycle represented a tool path that proceeded through angles of 0°, 45°, -45°, and finally 0°. The tool path can be seen in Fig. 1b, where only motion 2 was performed. Data recording was the same as the linear testing. An example of the angle and torque results can be seen in Fig. 2b. This test was repeated at a 20 mm penetration depth on the right and left sides of each lumbar IVD between L<sub>1</sub> and L<sub>5</sub>. Torsional speeds of 2, 3, 4, 6, and 8°/s were compared on the right side of C1 L<sub>4</sub>L<sub>5</sub>. Test details are shown in Table 2.

**Data analysis.** The data were then analyzed for comparison. Initial position, angle, force, and torque were normalized at the start of each test. This applied to all linear tests, but notably only the first torsional test. After extracting the relevant parameters, a variety of statistical comparisons were performed to determine the significance of differences between cadavers (C1, C2), lumbar levels (L<sub>1</sub>L<sub>2</sub>, L<sub>2</sub>L<sub>3</sub>, L<sub>3</sub>L<sub>4</sub>, L<sub>4</sub>L<sub>5</sub>), and tool passes (1, 2,

Statistical comparison of testing conditions					
Linear tests					
Comparison	Cadavers	Lumbar level	Pass number	Linear speed	Torsional speed
Force peak					
All passes	1.46E-01	7.23E-02	<b>2.05E-03</b>	<b>1.56E-02</b>	<b>2.16E-02</b>
Pass 1	5.74E-01	1.35E-01	–	–	–
Pass 2–3	<b>2.05E-02</b>	1.52E-01	*3.00E-01	8.33E-02	1.04E-01
Test method	Mann–Whitney U	Kruskal–Wallis			
Linear resistance					
All passes	2.36E-01	1.58E-01	<b>1.49E-03</b>	<b>2.16E-02</b>	<b>1.88E-02</b>
Pass 1	4.42E-01	1.13E-01	–	–	–
Pass 2–3	<b>3.32E-02</b>	2.49E-01	*3.76E-01	8.33E-02	8.33E-02
Test method	Mann–Whitney U	Kruskal–Wallis			
Torsion tests					
Comparison	Cadavers	Depth	Lumbar level	Pass number	Torsional speed
Torque peak					
All passes	<b>1.17E-05</b>	<b>5.69E-15</b>	<b>2.11E-10</b>	<b>1.63E-02</b>	<b>1.19E-03</b>
Pass 1	<b>2.13E-02</b>	<b>1.49E-05</b>	<b>4.71E-02</b>	–	2.12E-01
Pass 2–5	<b>1.93E-04</b>	<b>2.24E-11</b>	<b>2.62E-09</b>	2.56E-01	<b>1.04E-02</b>
Test method	Mann–Whitney U	Kruskal–Wallis			
Torsional resistance					
All passes	<b>1.29E-04</b>	<b>8.78E-05</b>	<b>5.27E-09</b>	<b>1.42E-03</b>	5.79E-02
Pass 1	9.20E-02	<b>2.69E-03</b>	<b>3.74E-02</b>	–	6.82E-01
Pass 2–5	<b>2.09E-04</b>	<b>4.34E-03</b>	<b>1.04E-07</b>	6.42E-01	8.29E-02
Test method	Mann–Whitney U	Kruskal–Wallis			

**Table 3.** Statistical comparisons of testing conditions. All bolded, italicized values have significance  $p \leq 0.05$  and exceed the JND threshold of 7%. \*Performed with Mann–Whitney U Test.

3, (4, 5) of linear (0.25, 0.50, 0.75, 1.00 mm/s) and torsional speed (10, 20, 30, 40°/s). Additional comparisons of penetration depth (5, 20 mm) and torsional speed (2, 3, 4, 6, 8°/s) were performed on the torsional tests. A Mann–Whitney U test was used to compare two conditions, Kruskal–Wallis was used for tests with three or more conditions, and data were compared to IVD height using Spearman correlation after confirming they were not normally distributed using a Shapiro–Wilk normality test<sup>46–49</sup>. Comparisons are summarized in Table 3, where bold, italicized values have a significance of  $\alpha \leq 0.05$ .

For linear tests, 11.5 mm of tool travel after the initial set position of 5 mm inside the IVD was used. A linear fit was performed on force versus position for the range of [0,11.5] mm, and the peak force at  $11.5 \pm 0.25$  mm was extracted. A sample fit is shown in Fig. 2a.

For torsional tests, the first  $\pm 20^\circ$  of tool rotation was used. A linear fit was performed on torque versus angle for the range of  $[0, \pm 20]^\circ$  and the peak torque at  $\pm 20 \pm 0.2^\circ$  ( $\pm 10$  data points at 100 Hz) was extracted. A sample fit is shown in Fig. 2b.

## Results

Data and overall comparisons were considered separately with force in the linear tests and torque in the torsional tests.

**Force. Peak.** Peak force samples can be seen for multiple conditions in Fig. 3 Average peak force at 11.5 mm was  $25.2 \pm 16.7$  N. There was a statistically significant difference between passes (P1, P2, P3). However, after the initial pass (P1), later passes (P2, P3) were similar, indicating that the results stabilize after the initial destructive pass (P1). Additionally, after the initial pass (P1) there was a statistically significant difference between cadavers (C1, C2). There was a significant difference when performing the test at linear speeds (0.25, 0.50, 0.75, 1.00 mm/s) and torsional speeds (10, 20, 30, 40°/s) when considering all trials. Boxplots containing this information are contained in Fig. 3, with corresponding  $p$  values in Table 3.

**Resistance.** The linear resistance can be seen for multiple conditions in Fig. 3. Average resistance over the range [0,11.5] mm was  $2.1 \pm 1.6$  N/mm. All statistical differences match those observed for peak values. Boxplots containing this information are contained in Fig. 3, with corresponding  $p$  values in Table 3.

**Disc height correlations.** IVD height appeared to have no statistically significant correlation with either the peak or linear resistance as seen in Fig. 4a,b.

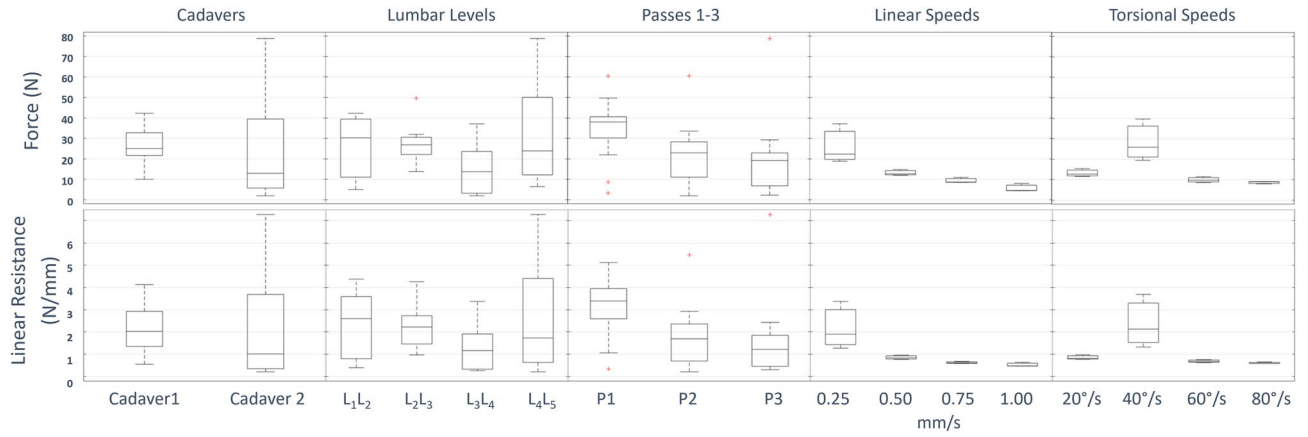


**Figure 3.** Force peak and linear resistance comparisons.

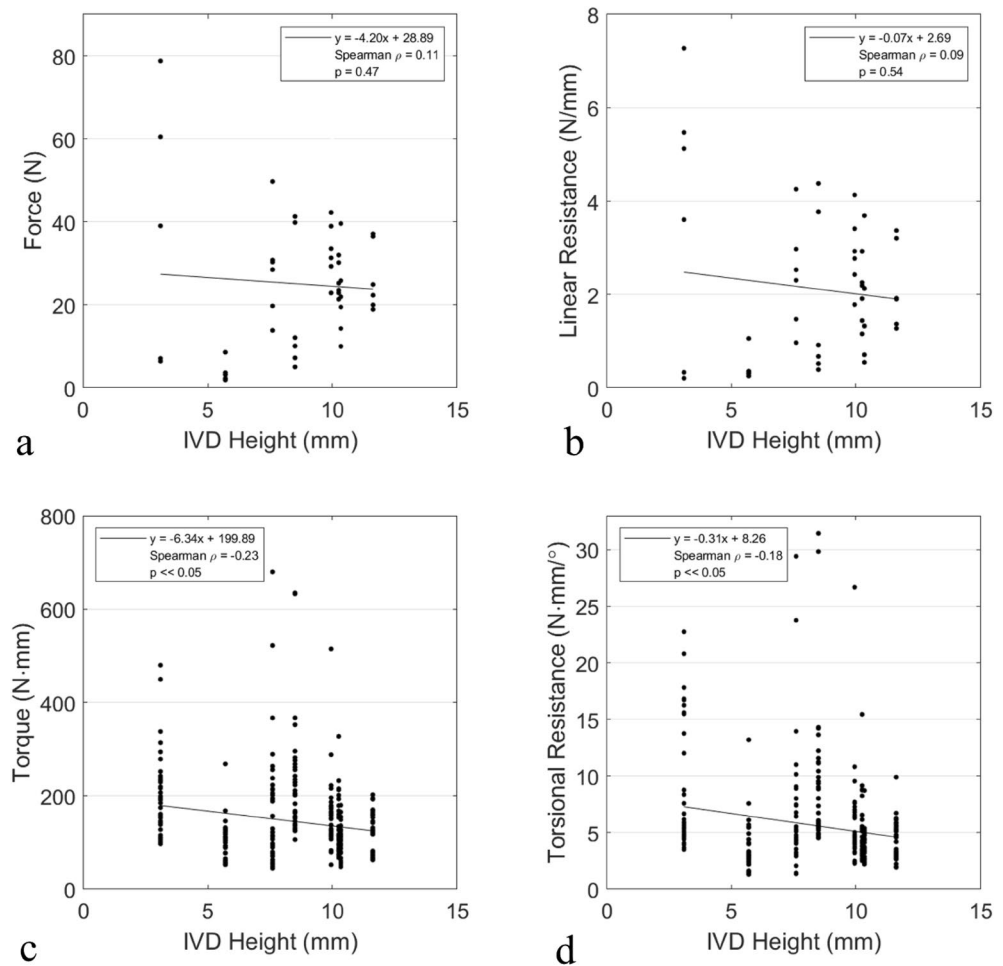


**Figure 4.** Linear (a,b) and torsional (c,d) peak and resistance values as correlated to intervertebral disc (IVD) height.

**Torque. Peak.** Peak torque samples can be seen in Fig. 5. Average torque magnitude at  $\pm 20^\circ$  was  $146.6 \pm 90.0$  N mm. Statistically significant differences were observed between cadavers (C1, C2), depths (5, 20 mm), lumbar levels ( $L_1L_2$ ,  $L_2L_3$ ,  $L_3L_4$ ,  $L_4L_5$ ), and passes (P1, P2, P3, P4, P5). For torsional speeds (2, 3, 4, 6, 8°/s), a difference was observed across all passes and after the initial pass (P1), but not for the initial pass (P1). Boxplots containing this information are shown in Fig. 5, with corresponding  $p$  values in Table 3.



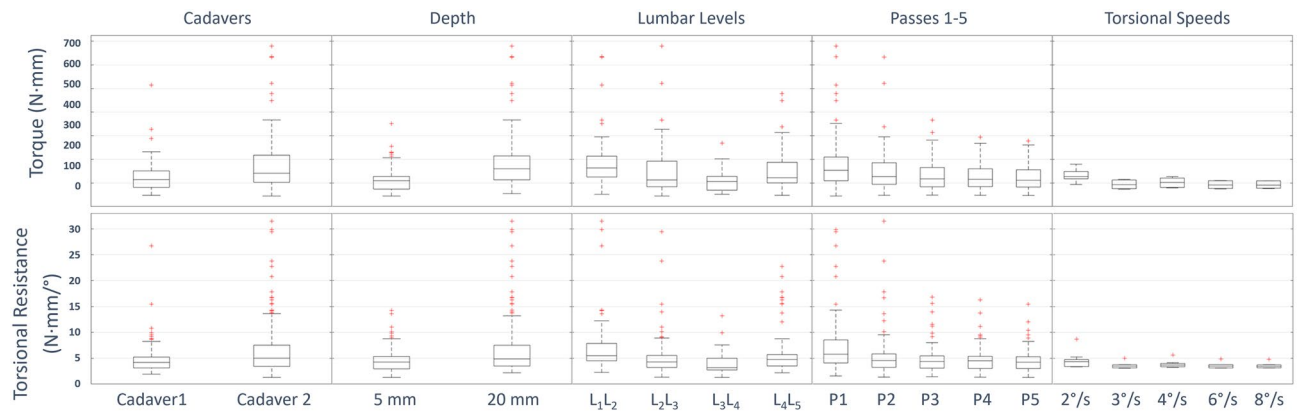


**Figure 5.** Torque peak and torsional resistance comparisons.

**Resistance.** The torsional resistance can be seen in Fig. 5. The average resistance on the range  $[0, 20]^\circ$  was  $5.6 \pm 4.3$  N mm/ $^\circ$ . All statistical differences matched those observed for the peak values, with the exceptions that differences between torsional speeds (2, 3, 4, 6, 8°/s) for any pass combination and the initial pass (P1) between cadavers (C1, C2) were not significant. Boxplots containing this information are contained in Fig. 5, with corresponding  $p$  values in Table 3.

**Disc height correlations.** IVD height appeared to have no statistically significant correlation with either the peak or torsional resistance, as seen in Fig. 4c,d.

## Discussion

The data presented show the range of expected force and torque present during a lumbar discectomy using the Concorde Clear. The hypothesis that force and torque would be dependent on spinal level and removed tissue at a  $\geq 7\%$  difference was confirmed in most cases. The difference between peak force and torque, as well as linear and torsional resistance, differed by  $\geq 7\%$  between initial and later passes through the tissue. Similar differences were found between lumbar levels, except for the peak force comparisons that did not meet the 7% threshold. To create a simulator or inform next generation discectomy tools, it is essential to identify how these data can be used to replicate or facilitate the surgical experience. This discussion focuses on distinguishing between anatomies or procedural conditions during the discectomy with respect to the JND of the user.

**Force.** Peak force at 11.5 mm and linear resistance over  $[0, 11.5]$  mm followed the same statistical patterns. The largest statistically significant difference across all conditions was between all passes (P1, P2, P3), with peak force decreasing after the initial pass (P1). This change suggests that the removal of tissue, or  $f_{cutting}$  in Eq. (1), was an essential distinguishing element during the procedure. However, after the initial pass (P1), the measured force for later passes (P2, P3) was the same. Variability in the initial pass (P1) was large enough that the difference between cadavers (C1, C2) was insignificant. However, after this destructive initial pass (P1), the cadaveric variation (C1, C2) became visible. Additionally, both linear and torsional speeds significantly impacted the force of insertion. In contrast, IVD height, which was used as an indicator of IVD degeneration, did not show a correlation with a change in force or linear resistance. This disconnect may be attributed to anatomical geometry. IVD height inside the disc was larger than around its perimeter, meaning the tool did not need to separate adjacent vertebrae away to penetrate deeper tissue after it had already penetrated the disc. Therefore, it can be considered that the most important factors to consider when designing a simulator for insertion of the Concorde Clear are the number of times the tool has passed through the disc and the speed at which the device is being pushed and twisted.

**Torque.** Peak torque at  $\pm 20^\circ$  and torsional resistance over  $[0, \pm 20]^\circ$  showed more statistical differences across comparisons than peak force and linear resistance. The peak torque was different between cadavers (C1, C2), penetration depths (5, 20 mm), and between all passes (P1, P2, P3, P4, P5), only being the same for the initial pass (P1) across the torsional speed (2, 3, 4, 6, 8°/s) tests. The torsional resistance was different across torsional speeds (2, 3, 4, 6, 8°/s) for all passes (P1, P2, P3, P4, P5), as well as the initial pass (P1) between cadavers (C1, C2). This suggests once again that the cutting torque, or other torque component only present in the initial pass, impacts the total torque significantly. Like the linear testing, both peak torque and torsional resistance were independent of IVD height and corresponding degeneration. While the tool did not need to further spread the IVD when penetrating, as in the force test, it did about the vertebral bodies during rotation. Adjacent IVDs may have accommodated this distraction by compressing and absorbing the torque, leading to similar results for all IVDs. However, the collapsed IVD (C2 L4L5), was included in this data set, and yet there was still no observed correlation. Greater variability between test conditions other than IVD height such as cadaver, pass number, and speed implies that more factors must be considered when designing torque output in a simulator than when designing the force output.

**Simulator application.** The data shown could be used to determine the appropriate force and torque needed in a Concorde Clear discectomy simulator. However, it was still necessary to determine if a user could distinguish between the statistically different conditions outlined above and in Table 3. Using a JND of 7%, as previously suggested, all statistically significant differences in peak force, peak torque, linear resistance, and torsional resistance shown in Table 3 would be detected by the surgeon. This implies that cadaveric differences, pass number, linear speed, and torsional speed should all be considered when determining the robotic force output, while lumbar level should not. Furthermore, cadaveric differences, tool depth, lumbar level, pass number, and torsional speed in some circumstances should be accounted for when determining the robotic torque output.

**Limitations.** As with any study, there were limitations to its scope. One key shortcoming of this work was that only the tool travel was measured, not the displacement of the body. This means that for a given tool displacement, the actual penetration of the tool into the IVD was less. The cadaveric torso was intentionally allowed to move slightly within its jig to replicate the compression or movement a surgeon may experience during surgery. This setup introduced more variability into the study, as the specific orientation and support of the sample will have an impact on the test. This restricted the applicability of the study to determine material properties of the IVD but was necessary to replicate surgical conditions. This is why the peak and resistance values for both force and torque were used, as well as the aggregated subcomponents of each as shown in Eq. (1) and previous work<sup>23</sup>. Another limitation was the impact of IVD height on beginning the discectomy. Both versions of the Concorde Clear were inserted 5 mm into the disc space before beginning the linear or torsional tests, meaning that the difficulty of entering the IVD before removing tissue was not measured. Because all data were normalized at 5 mm penetration for the linear test, differences in this initial force to penetrate the IVD, which may be more difficult for short IVDs, were not considered. Similarly, the torsional tests were only normalized at the beginning of the cyclical testing and the act of normalizing these data for each loading cycle for each pass and direction could have affected the results. Using more samples could have prevented wear and tissue destruction from impacting the results when performing multiple tests on the same IVD, however, this is why the total sum of forces was considered in the study. Finally, the assumptions used here, of a 7% JND, were based on existing work. However, studies have also found that providing feedback, training, and frequency changes can have an impact on JND<sup>30</sup>. Additionally, visual feedback has also been shown to impact user JND<sup>50</sup>. It is possible that surgeons, through their extensive training, have developed greater sensitivity. This could be tested in the future in a manner comparable to previous work that found surgeon forces differed based on experience level<sup>51</sup>.

The force and torque profiles shown here can be used to inform a haptic robot to give feedback to a user or future tool design. Operator speed, number of passes, and patient differences should be considered when determining appropriate force and torque output. Lumbar level and tool depth should additionally be considered for proper torque output. By making these adjustments before and during the procedure, a simulator can be created to accurately mimic an MI LIF discectomy.

## Conclusions and future work

This work presents the first biomechanical study of MI discectomy using the Concorde Clear. A framework is provided for the measured force and torque, how they vary over time and between multiple conditions. Improvements in these measurements could be made by quantifying the amount of tissue removed and correlating it to the measured mechanics. This would enable better modeling for the force output by allowing the simulator to respond to tissue removal as the user proceeds through a procedure. Following simulator development, studies must be performed with surgeons to evaluate how experts perceive the mechanics that have been measured and subsequently integrated. Perhaps surgeon JND differs from that of the normal population and therefore the simulator must be sensitive to minute differences between tissues in the procedure. This would validate the study results by showing how effective these data are in a simulator that is both biomechanically accurate and relevant for training. Overall, this study provides a better understanding of the force and torque encountered by a surgeon using a tool, such as the Concorde Clear, during a lumbar discectomy, and how these measures can be applied in a simulated environment.

## Data availability

The datasets used and analysed during the current study are available from M.D. on reasonable request.

Received: 12 April 2022; Accepted: 26 July 2022

Published online: 06 August 2022

## References

- Sweet, R. The CREST simulation development process: training the next generation. *J. Endourol.* **31**, S69–S75 (2017).
- Ruikar, D., Hegadi, R. & Santosh, K. A systematic review on orthopedic simulators for psycho-motor skill and surgical procedure training. *J. Med. Syst.* **42**(168), 1–21 (2018).
- Cooper, J. & Taqueti, V. A brief history of the development of mannequin simulators for clinical education and training. *Qual. Saf. Health Care* **13**, i11–i18 (2004).
- Go, T., Bürki-Cohen, J. & Soja, N. The effect of simulator motion on pilot training and evaluation. *Model. Simul. Technol. Conf.* <https://doi.org/10.2514/6.2000-4296> (2000).
- Casutt, G., Theill, N., Martin, M., Keller, M. & Jäncke, L. The drive-wise project: Driving simulator training increases real driving performance in healthy older drivers. *Front. Aging Neurosci.* **6**(86), 1–14 (2014).
- Alotaibi, F. E. *et al.* Utilizing NeuroTouch, a virtual reality simulator, to assess and monitor bimanual performance during brain tumor resection. *Can. J. Neurol. Sci.* **42**(S1), S20–S20 (2015).
- Alotaibi, F. *et al.* Assessing bimanual performance in brain tumor resection with neurotouch, a virtual reality simulator. *Neurosurgery* **11**, 89–98 (2015).



8. Winkler-Schwartz, A. *et al.* Machine learning identification of surgical and operative factors associated with surgical expertise in virtual reality simulation. *JAMA Netw. Open* **2**(e198363), 1–16 (2019).
9. Nikolaidis, N., Marras, I., Mikrogeorgis, G., Lyroutdia, K. & Pitas, I. Virtual dental patient: A 3D oral cavity model and its use in haptics-based virtual reality cavity preparation in endodontics. *Dent. Comput. Appl. Adv. Tech. Clin. Dent.* <https://doi.org/10.4018/978-1-60566-292-3.ch018> (2008).
10. Klein, S., Whyne, C., Rush, R. & Ginsberg, H. CT-based patient-specific simulation software for pedicle screw insertion. *J. Spinal Disord. Tech.* **22**, 502–506 (2009).
11. Akhtar, K., Chen, A., Standfield, N. & Gupte, C. The role of simulation in developing surgical skills. *Curr. Rev. Musculoskelet. Med.* **7**, 155–160 (2014).
12. Torkington, J., Smith, S., Rees, B. & Darzi, A. The role of simulation in surgical training. *Ann. R. Coll. Surg. Engl.* **82**, 88–94 (2000).
13. Kurashima, Y. *et al.* A novel low-cost simulator for laparoscopic inguinal hernia repair. *Surg. Innov.* **18**, 171–175 (2011).
14. Delorme, S., Laroche, D., Diraddo, R. & Del Maestro, R. NeuroTouch: A Physics-based virtual simulator for cranial microneurosurgery training. *Neurosurgery* **71**, 32–42 (2012).
15. Wang, Q. *et al.* Haptic rendering of drilling process in orthopedic surgical simulation based on the volumetric object. In: *Proceedings of the International Conference on Digital Signal Processing, DSP* vol. 2015 1098–1101 (Institute of Electrical and Electronics Engineers Inc., 2015).
16. Fuerst, D., Hollensteiner, M. & Schrepf, A. Assessment parameters for a novel simulator in minimally invasive spine surgery. In: *Proceedings of the Annual International Conference of the IEEE Engineering in Medicine and Biology Society, EMBS* 5110–5113 (2015). <https://doi.org/10.1109/EMBC.2015.7319541>.
17. Carfango, J. How osso VR is reshaping the surgical training process - docwire news. *DocWire News* <https://www.docwirenews.com/docwire-pick/future-of-medicine-picks/how-osso-vr-is-reshaping-the-surgical-training-process/> (2019).
18. Luciano, C. *et al.* Percutaneous spinal fixation simulation with virtual reality and haptics. *Neurosurgery* **72**, 89–96 (2013).
19. Instron. Modulus of Elasticity. <https://www.instron.com/en/our-company/library/glossary/m/modulus-of-elasticity>.
20. Ben-Ur, Z., Mijiritsky, E., Gorfil, C. & Brosh, T. Stiffness of different designs and cross-sections of maxillary and mandibular major connectors of removable partial dentures. *J. Prosthet. Dent.* **81**, 526–532 (1999).
21. Arruda, E. & Boyce, M. A three-dimensional constitutive model for the large stretch behavior of rubber elastic materials. *J. Mech. Phys. Solids* **41**, 389–412 (1993).
22. Cardenas, R. *et al.* Comparison of allograft bone and titanium cages for vertebral body replacement in the thoracolumbar spine: A biomechanical study. *Neurosurgery* **66**, 314–318 (2010).
23. Okamura, A., Simone, C. & O’Leary, M. Force modeling for needle insertion into soft tissue. *IEEE Trans. Biomed. Eng.* **51**, 1707–1716 (2004).
24. Penfield, W. & Boldrey, E. Somatic motor and sensory representation in the cerebral cortex of Mman as studied by electrical stimulation. *Brain* **60**, 389–443 (1937).
25. Kopta, J. The development of motor skills in orthopaedic education. *Clin. Orthop. Relat. Res.* **75**, 80–85 (1971).
26. Sadideen, H., Alvand, A., Saadeddin, M. & Kneebone, R. Surgical experts: Born or made?. *Int. J. Surg.* **11**, 773–778 (2013).
27. Pang, X., Tan, H. & Durlach, N. Manual discrimination of force using active finger motion. *Percept. Psychophys.* **49**, 531–540 (1991).
28. Allin, S., Matsuoka, Y. & Klatzky, R. Measuring just noticeable differences for haptic force feedback: Implications for rehabilitation. In *Proceedings of the 10th Symposium on Haptic Interfaces for Virtual Environment and Teleoperator Systems, HAPTICS 2002* 299–302 (2002). <https://doi.org/10.1109/HAPTIC.2002.998972>.
29. Zoeller, A. & Drewing, K. A systematic comparison of perceptual performance in softness discrimination with different fingers. *Attent. Percept. Psychophys.* **82**, 3696–3709 (2020).
30. Omrani, M., Lak, A. & Diamond, M. Learning not to feel: Reshaping the resolution of tactile perception. *Front. Syst. Neurosci.* **7**(29), 1–13 (2013).
31. Vicentini, M. & Botturi, D. Perceptual issues improve haptic systems performance. In: *Advances in Haptics* (ed. Zadeh, M. H.) 415–438 (InTech, 2010). <https://doi.org/10.5772/8711>.
32. Corey, D. & Comeau, D. Cervical radiculopathy. *Med. Clin. North Am.* **98**, 791–799 (2014).
33. Edelson, J. & Nathan, H. Nerve root compression in spondylolysis and spondylolisthesis. *J. Bone Joint Surg.* **68**, 596–599 (1986).
34. Takahashi, K., Shima, I. & Porter, R. Nerve root pressure in lumbar disc herniation. *Spine (Phila Pa 1976)* **24**, 2003–2006 (1999).
35. Rubin, D. Epidemiology and risk factors for spine pain. *Neurol. Clin.* **25**, 353–371 (2007).
36. Hoy, D. *et al.* The global burden of low back pain: Estimates from the Global Burden of Disease 2010 study. *Ann. Rheum. Dis.* **73**, 968–974 (2014).
37. Mobbs, R., Phan, K., Malham, G., Seex, K. & Rao, P. Lumbar interbody fusion: Techniques, indications and comparison of interbody fusion options including PLIF, TLIF, MI-TLIF, OLIF/ATP, LLIF and ALIF. *J. Spine Surg.* **1**, 2–18 (2015).
38. Mobbs, R., Sivabalan, P., Li, J., Wilson, P. & Rao, P. Hybrid technique for posterior lumbar interbody fusion: A combination of open decompression and percutaneous pedicle screw fixation. *Orthop. Surg.* **5**, 135–141 (2013).
39. Regan, J., Yuan, H. & McAfee, P. Laparoscopic fusion of the lumbar spine: minimally invasive spine surgery: A prospective multicenter study evaluating open and laparoscopic lumbar fusion. *Spine (Phila Pa 1976)* **24**, 402–411 (1999).
40. Mo, F., Yuan, P., Araghi, A. & Serhan, H. Time savings and related economic benefits of suction-curette device for transforaminal lumbar interbody fusion discectomy. *Int. J. Spine Surg.* **12**, 582–586 (2018).
41. Patwardhan, A., Havey, R., Meade, K., Lee, B. & Dunlap, B. A follower load increases the load-carrying capacity of the lumbar spine in compression. *Spine (Phila Pa 1976)* **24**, 1003–1009 (1999).
42. Shan, Z. *et al.* Correlation between biomechanical properties of the annulus fibrosus and magnetic resonance imaging (MRI) findings. *Eur. Spine J.* **24**, 1909–1916 (2015).
43. Hirsch, C. & Nachemson, A. New observations on the mechanical behavior of lumbar discs. *Acta Orthop. Scand.* **23**, 254–283 (1954).
44. La Barbera, L. *et al.* Load-sharing biomechanics of lumbar fixation and fusion with pedicle subtraction osteotomy. *Sci. Rep.* **11**(3595), 1–13 (2021).
45. El-Monajjed, K. & Driscoll, M. Analysis of surgical forces required to gain access using a probe for minimally invasive spine surgery via cadaveric-based experiments towards use in training simulators. *IEEE Trans. Biomed. Eng.* **68**, 330–339 (2021).
46. Mann, H. & Whitney, D. On a test of whether one of two random variables is stochastically larger than the other. *Ann. Math. Stat.* **18**, 50–60 (1947).
47. Kruskal, W. & Wallis, W. Use of ranks in one-criterion variance analysis. *J. Am. Stat. Assoc.* **47**, 583–621 (1952).
48. Gibbons, J. & Chakraborti, S. Spearman’s coefficient of rank correlation. In: *Nonparametric Statistical Inference* (ed. Dekker, M.) 422–432 (2003).
49. BenSaida, A. Shapiro-Wilk and Shapiro-Francia normality tests. *MATLAB Central File Exchange* <https://www.mathworks.com/matlabcentral/fileexchange/13964-shapiro-wilk-and-shapiro-francia-normality-tests> (2021).
50. Matsuoka, Y., Brewer, B. & Klatzky, R. Using visual feedback distortion to alter coordinated pinching patterns for robotic rehabilitation. *J. Neuroeng. Rehabil.* **4**(17), 1–9 (2007).
51. Ledwos, N. *et al.* Virtual reality anterior cervical discectomy and fusion simulation on the novel sim-ortho platform: validation studies. *Oper. Neurosurg.* **20**, 74–82 (2021).

## Acknowledgements

The authors would like to thank Dr. Rodrigo Navarro-Ramirez, who helped with cadaveric preparation, dissection, and test method setup. Funding and guidance were provided by CAE Healthcare, Inc. (Montreal, Canada) and DePuy Synthes. Testing was performed at Laboratoire de Recherche en Imagerie et Orthopedie division de l'Hôpital du Sacré-Coeur de Montréal under Prof. Yvan Petit and Prof. Eric Wagnac, with assistance from Ms. Elisabeth Laroche. Dr. Khaled El-Monajjed and Ms. Sneha Patel also assisted in the test design and execution.

## Author contributions

Test design and execution, analysis, and writing, T.C.; research guidance and review, M.D, R.M.

## Funding

The work was supported in part by the Natural Sciences and Engineering Research Council (NSERC), the Quebec Consortium for Industrial Research and Innovation in Medical Technology (MEDTEQ), DePuy Synthes, CAE Healthcare, Inc., and McGill University under Grant CRDPJ 515768–17.

## Competing interests

The authors declare no competing interests.

## Additional information

**Correspondence** and requests for materials should be addressed to M.D.

**Reprints and permissions information** is available at [www.nature.com/reprints](http://www.nature.com/reprints).

**Publisher's note** Springer Nature remains neutral with regard to jurisdictional claims in published maps and institutional affiliations.



**Open Access** This article is licensed under a Creative Commons Attribution 4.0 International License, which permits use, sharing, adaptation, distribution and reproduction in any medium or format, as long as you give appropriate credit to the original author(s) and the source, provide a link to the Creative Commons licence, and indicate if changes were made. The images or other third party material in this article are included in the article's Creative Commons licence, unless indicated otherwise in a credit line to the material. If material is not included in the article's Creative Commons licence and your intended use is not permitted by statutory regulation or exceeds the permitted use, you will need to obtain permission directly from the copyright holder. To view a copy of this licence, visit <http://creativecommons.org/licenses/by/4.0/>.

© The Author(s) 2022